03

# Modeling the boiling process of a liquid nitrogen jet outflow through a thin nozzle into a vacuum under cryogenic temperatures

© R.Kh. Bolotnova[1], E.F. Gainullina[1,2]

[1] Mavlyutov Institute of Mechanics UFRC RAS, Ufa, Russia
[2] Ufa University of Science and Technology, Ufa, Russia
E-mail: bolotnova@anrb.ru

*Received November 12, 2024*
*Revised November 28, 2024*
*Accepted November 28, 2024*

The process of liquid nitrogen jet outflow from a high-pressure vessel through a thin nozzle into a vacuum chamber is numerically investigated using the two-phase model of a vapor-liquid mixture in two-temperature, two-velocity, one-pressure approximations, taking into account non-equilibrium processes of evaporation and condensation. The wide-range equation of state in analytical form is used to describe the thermodynamic properties of the liquid and gas phases. Rate of mass transfer during evaporation is assumed to depend on the number and radius of bubbles, heat of vaporization, and degree of superheating. Features of the velocity field, formed by the expanding jet flow for the degree of superheat by pressure of 60, are considered. The obtained calculated velocity distribution of the boiling jet flow is in satisfactory agreement with the experimental data.

**Keywords:** boiling jet of liquid nitrogen, cryogenic temperatures, vacuum chamber, numerical simulation.

DOI: 10.61011/TPL.2025.04.60990.20181

The issues of cryogenic boiling liquid outflow from nozzles are an important area of experimental and theoretical research, since an understanding of these processes is crucial for the design of rocket engines in the context of ensuring their reliability and operating efficiency. Low boiling temperatures of liquids make it significantly harder to perform experiments in such regimes. New experimental data characterize in detail the dynamics of boiling of liquid nitrogen jets [1–3], which is important for modeling and studying the processes under examination, as well as for verifying the available models of vapor-liquid media [4–6]. The present study is a continuation of a series of original works [5,6] where the regimes of cryogenic liquid nitrogen outflow were examined experimentally under various degrees of superheat [1]. A developed by authors two-phase model of a vapor-liquid mixture was used in it. Unlike [5,6], this model includes a new wide-range analytical equation of state of nitrogen for liquid and gas phases [7]. The model was implemented numerically in the form of a new solver in the OpenFOAM [8] software. The features of forming velocity fields and distributions of the volumetric droplet content in an expanding jet flow were investigated for a degree of superheat $R_p = p_s(T_{inj})/p_c = 60$ higher than the one in [5,6]. Here, $p_s(T_{inj})$ is the saturation pressure at temperature $T_{inj}$ in the high-pressure chamber and $p_c$ is the backpressure in the vacuum chamber. Experiments with such flow regimes were carried out in [1,3] using the setup shown schematically in Fig. 1. Its geometric dimensions used in model calculations are listed in Table 1. The initial conditions set in the experiments chosen for study [1,3] are presented in Table 2. The outflow of a boiling jet was imaged in experiment [1] (see the corresponding conditions in Table 2) at a time of 120 ms (Fig. 2, *a*) using high-speed schlieren photography. The measurements of the spatial distribution of droplet velocities were performed in [3] under conditions 2 (Table 2) using a phase Doppler anemometry (PDA) system (Fig. 3). It was assumed in [1,3] that the conditions of experiments 1 and 2 (Table 2) were the same within reasonable error; therefore, it is fair to conduct a joint analysis of both experiments 1 and 2.

The main equations of the two-phase spatial model of a vapor-liquid mixture in two-temperature, two-velocity, and one-pressure approximations with account for contact heat transfer and nonequilibrium mass-transfer processes of evaporation and condensation [9,10] are as follows:

mass conservation equations for phase $i$

$$\frac{\partial(\alpha_i\rho_i)}{\partial t} + \mathrm{div}(\alpha_i\rho_i\mathbf{v}_i) = J_{ij}, \tag{1}$$

momentum conservation equations for phase $i$

$$\frac{\partial(\alpha_i\rho_i\mathbf{v}_i)}{\partial t} + \mathrm{div}(\alpha_i\rho_i\mathbf{v}_i\mathbf{v}_i) = \\ -\alpha_i\nabla p + \mathrm{div}(\alpha_i\tau_i) + \mathbf{F}_{i,drag} + \mathbf{F}_{i,vm} + J_{ij}\mathbf{v}_i, \tag{2}$$

and total energy conservation equations for phase $i$

$$\frac{\partial(\alpha_i\rho_i E_i)}{\partial t} + \mathrm{div}(\alpha_i\rho_i E_i\mathbf{v}_i) = \\ = -p\frac{\partial\alpha_i}{\partial t} - \mathrm{div}(\alpha_i\mathbf{v}_i p) - \mathrm{div}(\alpha_i\mathbf{v}_i\cdot\tau_i) \\ + \mathrm{div}(\alpha_i\gamma_{i,eff}\nabla h_i) + K_{ht}(T_j - T_i) + l_s J_{ij}. \tag{3}$$

The virtual mass force is

$$\mathbf{F}_{i,vm} = 0.5\alpha_l\rho_g\left(\frac{d_i\mathbf{v}_i}{dt} - \frac{d_j\mathbf{v}_j}{dt}\right).$$

**Table 1.** Geometric dimensions of the setup [1,3]

| Dimension | High-pressure chamber | Intermediate pipeline | Conical nozzle | Vacuum chamber |
|---|---|---|---|---|
| Length $x$, m | 0.136 | 0.12 | 0.03 | 0.225 |
| Radius $y$, m | 0.034 | $7 \cdot 10^{-3}$ | $0.5 \cdot 10^{-3}$ | 0.15 |

**Table 2.** Initial conditions of the simulated experiments [1,3]

| Experiment | Temperature $T_{inj}$ in the high-pressure chamber, K | Pressure $p_{inj}$ in the high-pressure chamber, Pa | Backpressure $p_c$, Pa | Degree of superheat $R_p = p_s(T_{inj})/p_c$ |
|---|---|---|---|---|
| 1 [1] | 90.5 | $5.5 \cdot 10^5$ | $55 \cdot 10^2$ | 69 |
| 2 [3] | 89.7 | $4.4 \cdot 10^5$ | $73 \cdot 10^2$ | 60 |

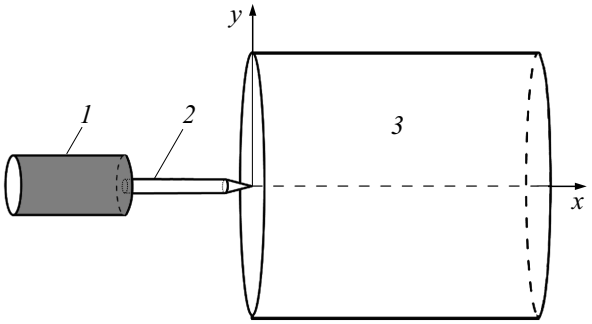


**Figure 1.** Diagram of the simulated experiment [1,3]. *1* — liquid nitrogen chamber, *2* — injector unit, and *3* — vacuum system.

The interfacial drag was characterized by the Schiller–Naumann model:

$$\mathbf{F}_{i,drag} = \frac{3}{4}\alpha_l C_D \frac{\rho_g}{d_{l0}}(\mathbf{v}_i - \mathbf{v}_j)|\mathbf{v}_i - \mathbf{v}_j|.$$

The following notation was used in Eqs. (1)–(3): $\rho_i$ is density, $T_i$ is temperature, $\alpha_i$ is volume content, $\mathbf{v}_i$ is the velocity vector, $J_{ij}$ is the rate of mass transfer between phases $i$ and $j$, $p$ is pressure, $\tau_i = \mu_i(\nabla\mathbf{v}_i + \nabla\mathbf{v}_i^T) - \frac{2}{3}(\mu_i \mathrm{div}\mathbf{v}_i)I$ is the viscous stress tensor, $\mu_i$ is dynamic viscosity, $E_i = e_i + K_i$ is the total energy in the form of a sum of internal and kinetic energies, $\gamma_{i,eff}$ is effective temperature conductivity, $h_i$ is enthalpy, $K_{ht} = \frac{\kappa_g}{d_{l0}}\mathrm{Nu}$ is the heat transfer coefficient, $\mathbf{v} = \alpha_l\mathbf{v}_l + \alpha_g\mathbf{v}_g$ is the velocity vector of a vapor-liquid mixture, $\kappa_g$ is the thermal conductivity of gas, $d_{l0}$ is the droplet diameter, Nu is the Nusselt number, and $l_s$ is the heat of vaporization/condensation. Lower indices $i$, $j = 1, 2$ correspond to the liquid $(l)$ and gas $(g)$ phases $(i \neq j)$.

The thermodynamic properties of vapor and liquid phases of nitrogen were characterized by the wide-range equation of state [7] in the form of a sum of elastic and thermal components of pressure and internal energy: $p = p_p + p_T$, $e = e_p + e_T$,

$$p_p(\rho_i) = A\left(\frac{\rho_i}{\rho_0}\right)^{-\beta+1} \exp\left[b\left(1 - \left(\frac{\rho_i}{\rho_0}\right)^{-\beta}\right)\right] - K\left(\frac{\rho_i}{\rho_0}\right)^{\varphi+1},$$

$$\rho_i = \frac{1}{V_i},\ p_T(V_i, T_i) = \frac{\Gamma_i(V_i)c_{Vi}}{V_i}T_i,$$

$$e_p(\rho_i) = \int_{\rho^0}^{\rho_i} \frac{p_p(\rho_i)}{\rho_i^2}d\rho = \frac{A}{\beta\rho_0 b}\exp\left[b\left(1 - \left(\frac{\rho_i}{\rho_0}\right)^{-\beta}\right)\right]$$

$$-\frac{K}{\varphi\rho_0}\left(\frac{\rho_i}{\rho_0}\right)^{\varphi} + e^{\circ},\ e_{Ti} = c_V T_i. \qquad (4)$$

Here, $A$, $K$, $b$, $\varphi$, and $\beta$ are constants specifying the elastic components of the equation of state; $c_{Vi}$ is isochoric heat capacity, $e^{\circ}$ is an integration constant, and $\Gamma_i(V_i)$ is the Grüneisen function [7].

Evaporation rate $J_{lg}$ was assumed to depend on number $n$ and radius $a$ of bubbles or droplets, saturation temperature $T_s(p)$, heat of vaporization $l_s(T)$, thermal conductivity coefficient of the liquid nitrogen phase $\lambda_l$, and Nusselt number Nu [11]:

$$J_{lg} = 2\pi a n \mathrm{Nu}\,\lambda_l\big(T - T_s(p)\big)/l_s(T). \qquad (5)$$

$\lambda_l = 1.12 \cdot 10^{-2}\,\mathrm{kg \cdot m/(s^3 \cdot K)}$ [8]. The approximation proposed by Labuntsov and obtained on the basis of Scriven's solution [11] was used for Nu:

$$\mathrm{Nu} = \frac{12}{\pi}\mathrm{Ja}\left[1 + \frac{1}{2}\left(\frac{\pi}{6\mathrm{Ja}}\right)^{2/3} + \frac{\pi}{6\mathrm{Ja}}\right],$$

$$\mathrm{Ja} = \frac{c_{pl}\big(T - T_s(p)\big)\rho_l^0}{l_s(T)\rho_g^0}$$

is the Jakob number and $c_{pl}$ is the specific heat capacity of liquid nitrogen at constant pressure. It was assumed that the liquid–vapor phase transition occurs under non-equilibrium super-heated conditions when the temperature

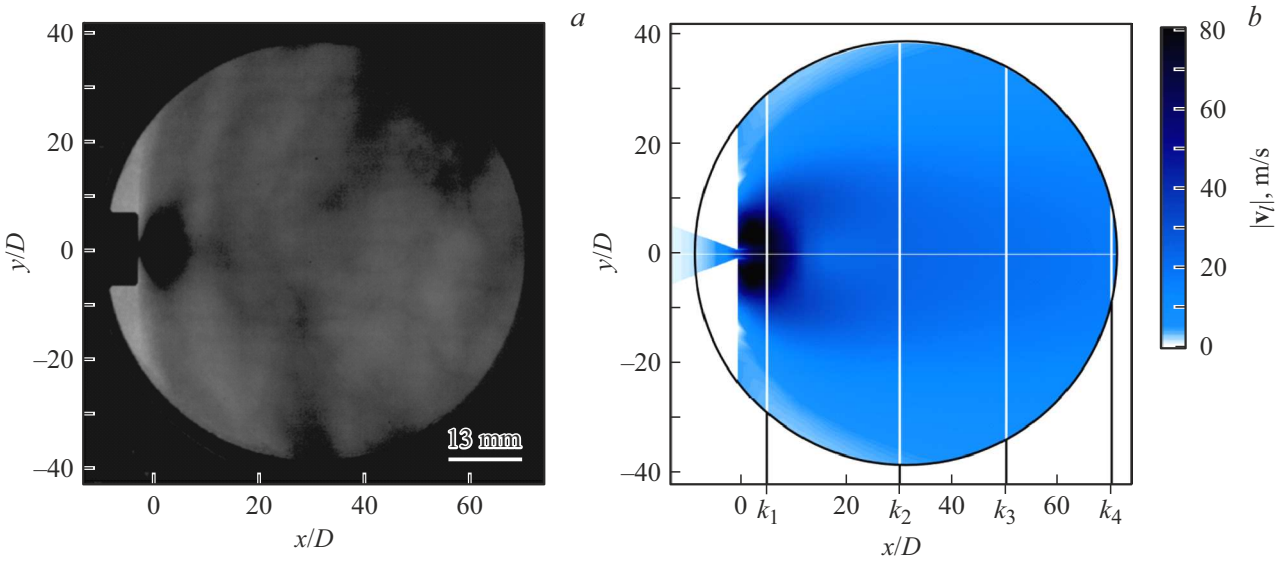


**Figure 2.** Comparison of the experimental photographic image [1] (*a*) and the calculated intensity distribution of the velocity field (*b*) for a liquid nitrogen jet at $t = 120$ ms and $R_p = 60$. $x/D = k_i$ — droplet velocity monitoring zones (see Fig. 3).

of the medium exceeds the saturation temperature [6,11]: $T > T_s(p) + \Delta T_s$, where $\Delta T_s$ is the degree of superheat of liquid by temperature that corresponds to the condition of pressure equilibrium in liquid and vapor with account for the capillary forces ($\Delta p_s \approx 2\sigma/a$) induced by surface tension $\sigma$ of the interphase surface [11]. At the initial stage of the non-equilibrium outflow process, the increase in $\alpha_g$ is attributable to the formation of new bubbles at inhomogeneous impurity particles. The growth of their radius is limited [11]: at $\alpha_g \leqslant 0.25$, the number of bubbles with radius $a = 6.5\,\mu$m is $n = 3\alpha_g/(4\pi a^3)$. At $\alpha_g > 0.25$, boiling proceeds in the equilibrium mode with a constant number of bubbles $n = 4 \cdot 10^{13}$ (in $1\,\text{m}^3$) with radius $a = \left(3\alpha_g/(4\pi n)\right)^{1/3}$. Further development of the process at $\Delta T_s = 0$ is characterized by an unlimited growth of the bubble radius, which, in accord with the experimental data [3], leads to the formation of a vapor-droplet system with droplet diameter $d = 10\,\mu$m.

Model (1)–(5) of the vapor-liquid mixture was implemented numerically in the OpenFOAM software [8] in the form of a new proprietary solver that is based on the control volume approach with the PIMPLE computational algorithm. The accuracy of numerical solutions was ensured by multi-block computational grids with refinement in the nozzle region ($\Delta x$, $\Delta y = 0.00001$–$0.006$ m) and by monitoring of the grid convergence until the stability of numerical solutions with initial time step $\Delta t = 1 \cdot 10^{-9}$ s was achieved.

The obtained numerical results and experimental data [1,3] are compared in Figs. 2, 3. Figure 2, *b* shows the calculated velocity magnitude distributions in the form of a color spectrum, which are qualitatively consistent with the photographic image obtained in experiment [1] (Fig. 2, *a*). An analysis of numerical solutions revealed that the forming jet at a time point of 120 ms has already entered a vapor-droplet outflow regime with droplet diameter $d_{l0} = 10\,\mu$m and is characterized by the maximum values of volumetric liquid content $\alpha_1 \approx 0.5$ in the nozzle mouth zone ($x/D = 0$–$5$). With increasing distance from the nozzle and away from the axis of symmetry, $\alpha_1$ decreases to 0.001 at $y/D = 150$. The average value of $\alpha_1$ in the central part of the jet is $\alpha_1 \approx 0.003$–$0.004$, which is indicative of a fairly uniform finely dispersed distribution of droplets in the vacuum chamber. Figure 3 shows the calculated distributions of droplet velocity magnitudes $|\mathbf{v}_l|$ at time $t = 120$ ms and the experimental points [3] at various distances along the axis of symmetry (see curve and points *1*) and in sections located at distances $x/D = k_i$, $i = 1, \ldots, 4$ from the nozzle (see curves and points *2*–*5*). The highest droplet velocities of $\sim 70$ m/s are found near the nozzle exit at $x/D = 5$ (see $k_1$ in Fig. 3). As one moves away from this zone along the axis of symmetry, the intensity of mass velocities decreases to $\sim 5$ m/s at $x/D = 70$ (see $k_4$ in Fig. 3) and $\sim 0.1$ m/s at $y/D = 150$. These calculations are in satisfactory agreement with the experimental data [3].

The processes of formation of an expanding jet outflow of liquid nitrogen into a vacuum chamber under the conditions of the chosen experiments were studied numerically based on the proposed two-phase vapor-liquid mixture model, and the obtained solutions were found to be accurate, which is verified by their satisfactory agreement with the experimental data. The simulation for initial degree of superheat $p_s(T_{inj})/p_c = 60$ at time $t = 120$ ms produced a fairly uniform finely dispersed distribution of droplets in the vacuum chamber, which differs from the results reported in [5,6] that were obtained by analyzing the water content fields at lower degrees of superheat. Such studies are

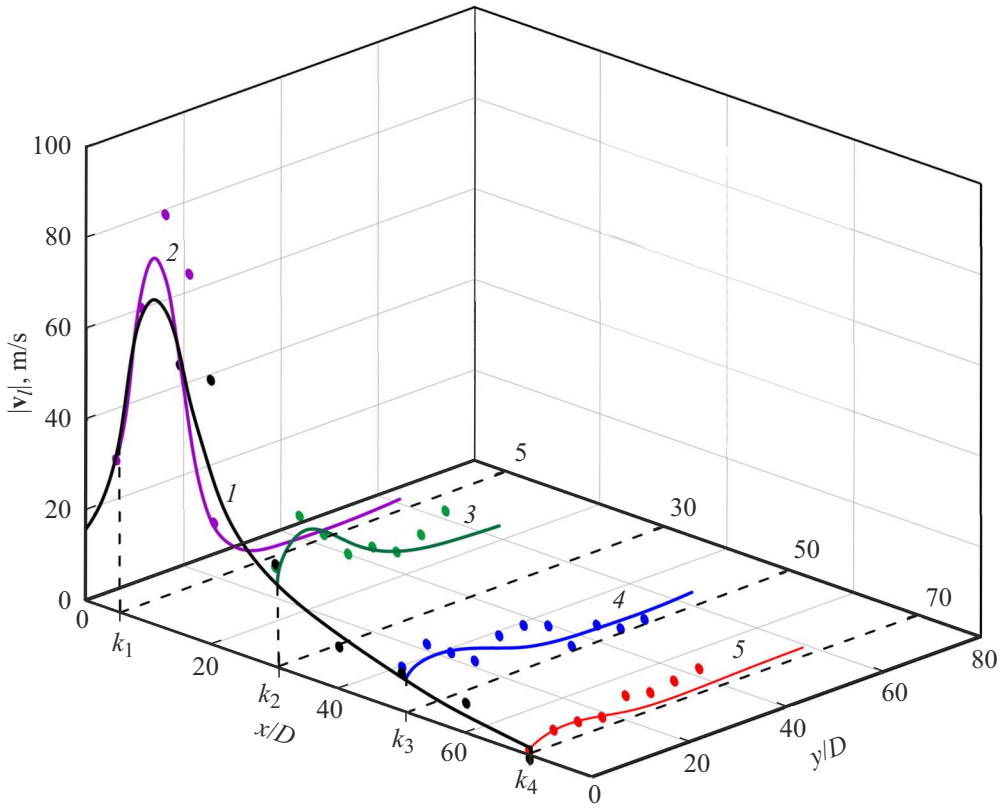


**Figure 3.** Calculated and experimental dependences of the droplet velocity magnitude distribution at time point $t = 120$ ms along the $y = 0$ symmetry axis (*1*) and in $x/D = k_i$ $(i = 1, \ldots, 4)$ sections away from the nozzle (*2–5*). Solid curves and symbols correspond to calculated and experimental data on droplet velocity [3].

of particular importance in the design of rocket engines operating at cryogenic temperatures and low pressures, since a detailed analysis of the distribution of fluid phases and the diameter and concentration of droplets in the vacuum chamber is aimed at determining the optimum operating regimes that contribute to an increase in the engine thrust.

## Funding

The research was financially supported by the state budget under the state task № 124030400064-2 (FMRS-2024-0001).

## Conflict of interest

The authors declare that they have no conflict of interest.

## References

[1] A. Rees, L. Araneo, H. Salzmann, E. Kurudzija, D. Suslov, G. Lamanna, J. Sender, M. Oschwald, in *29th ILASS-Europe Conf.* (Paris, France, 2019).
[2] A. Rees, H. Salzmann, J. Sender, M. Oschwald, in *8th Eur. Conf. for aeronautics and space sciences (EUCASS)* (Madrid, Spain, 2019). DOI: 10.13009/EUCASS2019-418
[3] A. Rees, L. Araneo, H. Salzmann, G. Lamanna, J. Sender, M. Oschwald, Exp. Fluids, **61**, 182 (2020). DOI: 10.1007/s00348-020-03020-7
[4] T. Lyras, I.K. Karathanassis, N. Kyriazis, P. Koukouvinis, M. Gavaises, Appl. Therm. Eng., **237**, 121773 (2024). DOI: 10.1016/j.applthermaleng.2023.121773
[5] R.Kh. Bolotnova, V.A. Korobchinskaya, E.F. Gainullina, Lobachevskii J. Math., **44** (5), 1579 (2023). DOI: 10.1134/S1995080223050104
[6] R.Kh. Bolotnova, V.A. Korobchinskaya, E.F. Gainullina, Tech. Phys. Lett., **49** (12), 108 (2023). DOI: 10.61011/TPL.2023.12.57601.107A.
[7] R.Kh. Bolotnova, E.F. Gainullina, V.A. Korobchinskaya, Lobachevskii J. Math., **44** (5), 1587 (2023). DOI: 10.1134/S1995080223050116
[8] *OpenFOAM. The Open source computational fluid dynamics (CFD) toolbox* [Electronic source]. http://www.openfoam.com
[9] R.I. Nigmatulin, *Dynamics of multiphase media* (Hemisphere, N.Y., 1990).
[10] L.D. Landau, E.M. Lifshitz, *Course of theoretical physics. Fluid mechanics* (Pergamon, N.Y., 1987).
[11] R.Kh. Bolotnova, V.A. Buzina, M.N. Galimzyanov, V.Sh. Shagapov, Teplofiz. Aeromekh., **19** (6), 719 (2012) (in Russian).

*Translated by D.Safin*